# Coriolis Effect on the Flow of Water Carrying CNT, Graphene, and Alumina Nanoparticles over a Heated Moveable Non-porous Surface

OLUWASEUN BIODUN ONUOHA[1], FAWWAZ BATAYNEH[2],
ABAYOMI SAMUEL OKE[3,*,a], MARIO RASO[4]

[1]Department of Mathematical Sciences, Adekunle Ajasin University, NIGERIA
[2]Mathematics Division, College of Engineering, Kuwait College of Science and Technology, Doha, KUWAIT
[3]Department of Mathematical Sciences, Adekunle Ajasin University, NIGERIA
[4]Department of Computer Science, Sapienza University of Rome, ITALY

[*]Corresponding Author
[a]ORCiD: 0000-0003-3903-4112

*Abstract:* Heat transfer fluids, heat exchangers, and coolants in electronics are typical industrial applications where improved fluids are required for optimal performance. Stemming from the increasing demand, this study examines the effects of suction, heat source and stretch- ing ratio on the flow and heat transfer in a magnetohydrodynamic ternary hybrid nanofluid across a moveable rotating surface. Carbon nanotubes, graphene and alumina are considered as the nanoparticles with water as the base fluid. The governing equations are transformed from partial to ordinary differential equations. The equilibrium point of the system was obtained, the conditions for the system stability were established and the emerging parameters were chosen within the acceptable interval. The equations are numerically solved using the MATLAB bvp4c solver. The effects of the flow parameters on the velocity and temperature distribution are graphically illustrated. The analysis shows that the stretching ratio reduces flow temperature and velocity but increases skin friction. Coriolis force enhances the heat transfer rate and increases the primary skin friction. Heat source increases flow temperature and secondary skin friction.

*Keywords:* Ternary hybrid nanofluid; Coriolis force; Heat source; Suction; Stretching ratio

Received: February 25, 2024. Revised: September 7, 2024. Accepted: October 8, 2024. Published: November 21, 2024.

MSC: 76U05, 76N20, 76A02

## 1. Background Information

The inability of most fluids to meet the industrial thermophysical requirements prompted Maxwell [1] to consider suspending solid particles, mostly millimetre-sized, in fluids. The development improved the thermal and electrical characteristics of the fluid but the solid particles, being heavy, settle at the wall and give rise to challenges such as clogging and pipe erosion. The suggestion of Choi and Eastman [2] to replace the millimetre-sized particle with a nanometre-sized particle revolutionised the study of fluid flow. The idea resolved the clogging and pipe erosion problem of Maxwell's approach [3, 4]. Since the innovation, authors have considered the suspension of more than one type of nanoparticle. Lee et al. [5] showed that the thermal conductivity of the base fluid increased by more than 20% when two nano-

particles were suspended in the base fluid and Baghbanzadeh et al. [6] showed that the heat transfer rate increased by 14%. Suresh et al. [7] considered the hybrid nanofluid of copper-alumina hybrid nanofluid, Hayat and Nadeem [8] studied silver-copper(II)oxide in water and Oke et al. [9] considered the flow of copper-alumina in water. Other recent studies on hybrid nanofluid can be found in [10, 11, 12]. Recently, it has been shown that ternary hybrid nanofluids enhance the thermal and electrical properties of the fluids better than the nanofluids or hybrid nanofluids [13]. Mousavi et al. [14] examined the impact of volume fraction and temperature on the thermophysical properties of a water-based ternary hybrid nanofluid of CuO, MgO, and TiO. The results showed an improvement in the thermal conductivity of the ternary hybrid nanofluid with increasing volume fraction. Furthermore, Elnaqeeb et al. [13] and Oke [15] considered the suspension of carbon nanotubes, graphenes and alumina in water. The study considered the effect of various particle shapes and sizes on the thermal properties of the fluid. The results show that temperature is enhanced at a small volume fraction.

Power generation, cancer tumour treatment and magnetic devices for cell separation are all practical applications where the use of magnetohydrodynamic (MHD) flows play vital roles. MHD flow becomes more applicable when the geometry of flow involves rotation as seen in ([16, 17, 18, 19, 15]). Oke et al. [20] explored the effect of rotating surfaces on the MHD flow of water and air. It was discovered that increasing surface rotation raises flow temperature and that increasing magnetic field strength counteracts the effects of increased Coriolis force on skin friction and heat transfer rate. Oyem et al. [21] considered the effects of variable thermal conductivity on an MHD Blasius and Sakiadis flows. The results show that velocity profiles reduce and the temperature increases with increasing magnetic field strength for both Sakiadis and Blasius flows. The impact of magnetic field on the transport of micropolar fluid was reported by Fatunmbi et al. [22]. Ouru et al. [23] showed that the magnetic field strength also inhibits the flow velocity and increases temperature profiles. The flow of a reactive tangent hyperbolic fluid over a non-linear stretching surface was evaluated by Fatunmbi et al. [24]. The authors pointed out that the momentum boundary layer and fluid velocity were reduced due to the drag-like Lorentz force occasioned by the magnetic field. Insightful results on the MHD flow of Eyring-Powell fluid over a stretching sheet with a convective boundary condition were shown in Oke and Mutuku [25]. Williamson fluid flow over an inclined rotating surface is studied in the presence of a magnetic field by Juma et al. [26].

Carbon is the fourth most abundant chemical element in the universe, following the gases hydrogen, helium, and oxygen [27]. As the most abundant solid element, carbon is an excellent candidate for use in nanoparticles within nanofluids. Carbon exists in several allotropes [28], including graphite, diamond, fullerenes, graphene, and carbon nanotubes. These allotropes have diverse industrial applications, such as steel production, where graphite is used for electrodes and lubricants, and diamonds for cutting tools and abrasives [29, 30]. Given their exceptional properties, this study focuses on the use of carbon nanotubes and graphene as nanoparticles in the nanofluids. From the literature above, studies have been carried out to consider the flow of ternary hybrid nanofluid over moveable surfaces. However, the studies have been restricted to nanoparticles of different shapes, and non-rotating surfaces and without considering heat source. These are the research gaps filled with this study where the flow of ternary hybrid nanofluid. (made from the suspension of carbon nanotube (CNT), alumina and graphene nanoparticles in water) over a rotating moveable surface under the influence of heat source. This study provides answers to the following research questions;

1. How can the flow parameters be chosen to sustain model stability?

2. what is the influence of the stretching ratio on the transport phenomenon of the flow of ternary hybrid nanofluid over a moveable rotating surface?

3. to what extent does channel rotation affect the heat transfer rate, skin friction and other transport properties of the flow of ternary-hybrid nanofluid over a moveable rotating surface?

4. how does the heat source affect the temperature, velocity, skin friction and heat transfer rate in the MHD flow of ternary hybrid nanofluid over a rotating surface?

## 2. Research Methodology

### 2.1 Mathematical Formulation

This study models the transport processes of a water-based ternary hybrid nanofluid that suspends three distinct nanoparticles of similar shapes in a moveable rotating channel. The flow is taken to be laminar and incompressible, subject to a magnetic field of constant magnetic field strength $B_0$. The surface produces the imaginary Coriolis force due to rotation with an angular velocity of $\Omega$. Assuming the flow adheres to the boundary layer theory [31] and the Sakiadis [32] theory on a moveable surface, the physical configuration of the flow is depicted in Figure (1). The fluid layers adhered to the surface obeyed the no-slip requirement, and the surface is extended linearly in the $xy$-plane. The $xy$- surface is assumed to move linearly while the fluid layers glued to the surface obey the no-slip condition. Hence, following the work of Elnaqeeb et al. [13], Oke et al. [33] and Oke [15], the flow can be modelled as the following equations;

$$\partial_x u + \partial_y v + \partial_z w = 0, \tag{1}$$

$$\left(u\partial_x + v\partial_y + w\partial_z\right) u = \frac{\mu_{tf}}{\rho_{tf}}\partial_{zz}u - 2\Omega u - \frac{\sigma_{tf}B_0^2}{\rho_{tf}}u, \tag{2}$$

$$\left(u\partial_x + v\partial_y + w\partial_z\right) v = \frac{\mu_{tf}}{\rho_{tf}}\partial_{zz}v + 2\Omega v - \frac{\sigma_{tf}B_0^2}{\rho_{tf}}v, \tag{3}$$

$$\left(u\partial_x + v\partial_y + w\partial_z\right) T = \alpha_{tf}\partial_{zz}T + \frac{Q_0}{\left(\rho C_p\right)_{tf}}\left(T_w - T_\infty\right)\exp\left(-z\sqrt{\frac{a}{\nu_{bf}}}\right). \tag{4}$$

At the base of the channel $(z = 0)$, the fluid layers on the wall admit the same velocity as that of the stretching wall and thus, the no-slip condition is retained as

$$\text{on the } x\text{-axis}: \quad u = ax,\ w = z_w - \left(a\nu_{bf}\right)^{\frac{1}{2}}\int \frac{v}{ay}d\eta.$$

$$\text{on the } y\text{-axis}: \quad v = ay,\ w = z_w - \left(a\nu_{bf}\right)^{\frac{1}{2}}\int \frac{u}{ax}d\eta,$$

$$\text{on the } (x,y)\text{-plane}, \ T = T_w.$$

Furthermore, at the free stream $(z \to \infty)$, the free stream conditions are sustained as

$$u \to 0, \ \text{ on the } x\text{-axis},$$
$$v \to 0, \ \text{ on the } y\text{-axis},$$
$$T = T_\infty \ \text{ on the } (x,y)\text{-plane}.$$

The characteristics of the flow that of practical implication are the skin drags and heat transfer rate in all directions which are defined as

$$C_{fx} = \mu_{tf}\left(\rho_{bf}a^2x^2\right)^{-1}\left.\frac{\partial u}{\partial z}\right|_{z=0}, \tag{5}$$

$$C_{gy} = \mu_{tf}\left(\rho_{bf}a^2y^2\right)^{-1}\left.\frac{\partial v}{\partial z}\right|_{z=0}, \tag{6}$$

$$Nu_x = -x\kappa_{tf}\left(\kappa_{bf}\left(T_w - T_\infty\right)\right)^{-1}\left.\frac{\partial T}{\partial z}\right|_{z=0}, \tag{7}$$

$$Nu_y = -y\kappa_{tf}\left(\kappa_{bf}\left(T_w - T_\infty\right)\right)^{-1}\left.\frac{\partial T}{\partial z}\right|_{z=0}. \tag{8}$$

Since the properties of the resulting ternary nanofluid properties are influenced by the properties of both the base fluid and the nanoparticles, the following definitions extracted from literature [33, 13] are adopted in this study

$$\mu_{tf} = \frac{1}{\phi}\sum_{j=1}^{3}\mu_j\phi_j, \ \kappa_{tf} = \frac{1}{\phi}\sum_{j=1}^{3}\kappa_j\phi_j, \tag{9}$$

$$\rho_{tf} = \left(1-\phi\right)\rho_{bf} + \sum_{j=1}^{3}\rho_j\phi_j \ \Rightarrow \ \rho_{tf} = \rho_{bf}A_1, \tag{10}$$

$$\left(\rho c_p\right)_{tf} = \left(1-\phi\right)\left(\rho c_p\right)_{bf} + \sum_{j=1}^{3}\left(\rho c_p\right)_j\phi_j$$
$$\Rightarrow \ \left(\rho c_p\right)_{tf} = \left(\rho c_p\right)_{bf}A_2$$

where

$$A_1 = 1 - \phi + \frac{1}{\rho_{bf}}\sum_{j=1}^{3}\rho_j\phi_j,$$

$$A_2 = 1 - \phi + \frac{1}{\left(\rho c_p\right)_{bf}}\sum_{j=1}^{3}\left(\rho c_p\right)_j\phi_j.$$

The thermophysical properties of the nanoparticles and the base fluid are provided in table (3). Also, the ternary nanofluid is made up of three different nanofluids. Considering platelet-shaped nanoparticles, then the viscosity and

thermal conductivity of the nanofluids are modelled as

$$\mu_j = \left(1 + 37.1\phi_j + 612.6\phi_j^2\right)\mu_{bf}$$
$$\frac{\kappa_j}{\kappa_{bf}} = \frac{\kappa_j + 4.7\kappa_{bf} - 4.7\phi\left(\kappa_{bf} - \kappa_j\right)}{\kappa_j + 4.7\kappa_{bf} + \phi\left(\kappa_{bf} - \kappa_j\right)}$$

for $j = 1, 2, 3$ and $\phi_j > 0.02$. Hence, with this model, we have

$$\begin{aligned}\mu_{tf} =& \frac{1}{\phi}\sum_{j=1}^{3}\mu_j\phi_j \\ =& \frac{\mu_{bf}}{\phi}\sum_{j=1}^{3}\left(1 + 37.1\phi_j + 612.6\phi_j^2\right)\phi_j \\ =& \frac{\mu_{bf}}{\phi}A_3 \qquad (11)\\ \kappa_{tf} =& \frac{1}{\phi}\sum_{j=1}^{3}\kappa_j\phi_j \\ =& \frac{\kappa_{bf}}{\phi}\sum_{j=1}^{3}\frac{\kappa_j + 4.7\kappa_{bf} - 4.7\phi\left(\kappa_{bf} - \kappa_j\right)}{\kappa_j + 4.7\kappa_{bf} + \phi\left(\kappa_{bf} - \kappa_j\right)}\phi_j \\ =& \frac{\kappa_{bf}}{\phi}A_4, \qquad (12)\end{aligned}$$

where

$$A_3 = \sum_{j=1}^{3}\left(1 + 37.1\phi_j + 612.6\phi_j^2\right)\phi_j,$$
$$A_4 = \sum_{j=1}^{3}\frac{\kappa_j + 4.7\kappa_{bf} - 4.7\phi\left(\kappa_{bf} - \kappa_j\right)}{\kappa_j + 4.7\kappa_{bf} + \phi\left(\kappa_{bf} - \kappa_j\right)}\phi_j.$$

## 2.2 Similarity Transformation

Employing the similarity variables

$$u = axf',\ v = acyg',\ w = -\left(a\nu_{bf}\right)^{\frac{1}{2}}\left(f + cg\right) \qquad (13)$$

$$T = T_\infty + \left(T_w - T_\infty\right)\theta,\ \eta = z\left(\frac{a}{\nu_{bf}}\right)^{\frac{1}{2}}, \qquad (14)$$

the equations are rendered dimensionless and the number of parameters is reduced to become

$$\frac{A_3}{\phi A_1}f''' + \left(f + cg\right)f'' - \left(f'\right)^2 - \left(K + \frac{M}{A_1}\right)f' = 0, \qquad (15)$$

$$\frac{A_3}{\phi A_1}g''' + \left(f + cg\right)g'' - c\left(g'\right)^2 + \left(K - \frac{M}{A_1}\right)g' = 0, \qquad (16)$$

$$\frac{A_4}{\phi A_2}\Theta'' + \frac{PrQ}{A_2}e^{-\eta} + Pr\left(f + cg\right)\Theta' \qquad (17)$$

with the boundary and initial conditions

$$\text{at } \eta = 0; \quad f = f_w,\ f' = 1,\ g = \frac{f_w}{c},\ g' = 1,\ \Theta = 1, \qquad (18)$$

$$\text{as } \eta \to \infty;\ f' \to 0,\ g' \to 0,\ \Theta \to 0. \qquad (19)$$

$$A_1 = 1 - \phi + \frac{1}{\rho_{bf}}\sum_{j=1}^{3}\rho_j\phi_j,$$
$$A_2 = 1 - \phi + \frac{1}{\left(\rho c_p\right)_{bf}}\sum_{j=1}^{3}\left(\rho c_p\right)_j\phi_j,$$
$$A_3 = \sum_{j=1}^{3}\left(1 + 37.1\phi_j + 612.6\phi_j^2\right)\phi_j,$$
$$A_4 = \sum_{j=1}^{3}\frac{\kappa_j + 4.7\kappa_{bf} - 4.7\phi\left(\kappa_{bf} - \kappa_j\right)}{\kappa_j + 4.7\kappa_{bf} + \phi\left(\kappa_{bf} - \kappa_j\right)}\phi_j.$$
$$K = \frac{2\Omega}{a},\ M = \frac{\sigma B_0^2}{a\rho_{bf}},\ Q = \frac{Q_0}{a\left(\rho c_p\right)_{bf}},$$
$$Pr = \frac{\nu_{bf}}{\alpha_{bf}},\ \alpha_{bf} = \frac{\kappa_{bf}}{\left(\rho c_p\right)_{bf}}.$$

The flow characteristics that are of practical interest are also reduced to

$$Re_x^{\frac{1}{2}}C_{fx} = \phi^{-1}A_1f''\left(0\right),\ Re_y^{\frac{1}{2}}C_{gy} = \phi^{-1}A_1g''\left(0\right) \qquad (20)$$

$$Re_x^{-\frac{1}{2}}Nu_x = Re_y^{-\frac{1}{2}}Nu_y = -\phi^{-1}A_3\Theta'\left(0\right). \qquad (21)$$

## 2.3 Method of Solution

The system of equations (15) - (17) has boundary conditions (18) and (19) which makes it difficult to adopt a direct numerical solution.

Hence, the shooting technique is required to convert the boundary conditions to initial conditions. To start with, equations (15) - (17) are rewritten as a system of first-order differential equations by setting

$$h_1 = f,\ h_2 = f',\ h_3 = f'',\ h_4 = g,\ h_5 = g',$$
$$h_6 = g'',\ h_7 = \Theta,\ h_8 = \Theta'$$

to have

$$h_1' = h_2, \tag{22}$$
$$h_2' = h_3, \tag{23}$$
$$h_3' = -\frac{\phi A_1}{A_3}\left[(h_1 + ch_4)\,h_3 - h_2^2 - \left(K + \frac{M}{A_1}\right)h_2\right], \tag{24}$$
$$h_4' = h_5, \tag{25}$$
$$h_5' = h_6, \tag{26}$$
$$h_6' = -\frac{\phi A_1}{A_3}\left[(h_1 + ch_4)\,h_6 - ch_5^2 + \left(K - \frac{M}{A_1}\right)h_5\right], \tag{27}$$
$$h_7' = h_8, \tag{28}$$
$$h_8' = -\frac{\phi A_2}{A_4}Pr\left[(h_1 + ch_4)\,h_8 + \frac{Q}{A_2}\exp(-\eta)\right]. \tag{29}$$

However, we have a combination of the initial and boundary conditions (18) and (19). The shooting technique requires that all these conditions be rewritten as initial conditions, by placing an arbitrary initial guess for the variables whose conditions are not known. In this case, we have the conditions as

$$h_1 = f_w,\ h_2 = 1,\ h_3 = \varepsilon_1,\ h_4 = \frac{f_w}{c}, \tag{30}$$
$$h_5 = 1,\ h_6 = \varepsilon_2,\ h_7 = 1,\ h_8 = \varepsilon_3. \tag{31}$$

where $\varepsilon_1, \varepsilon_2, \varepsilon_3$ are arbitrary guesses that will be updated after every iteration until the boundary conditions

$$h_2(\infty) = 0,\ h_5(\infty) = 0,\ h_7(\infty) = 0$$

are satisfied up to a specified tolerance level. The MATLAB bvp4c solver is used to solve the system (See Oke [34] for some other semi-analytical methods of solution). The bvp4c solver [35] executes the finite difference code that implements the three-stage Lobatto IIIa formula of the fourth order. The system is solved with an absolute tolerance of $10^{-4}$ and a relative tolerance of $10^{-4}$.

## 2.4 Qualitative analysis

The stability analysis of the equations (22 - 29) is carried out in this section. This becomes necessary to identify the range of values acceptable for the parameter values. By setting right hand side of the equations to 0, we have the equilibrium point as

$$(h_1, h_2, h_3, h_4, h_5, h_6, h_7, h_8) = \left(a_1, 0, 0, a_4, 0, 0, a_7, \frac{Q\exp(-\eta)}{A_2(a_1 + ca_4)}\right).$$

The characteristic equation obtained by substituting the equilibrium point into the Jacobian of the system is

$$\begin{vmatrix} -\lambda & 1 & 0 & 0 & 0 & 0 & 0 & 0 \\ 0 & -\lambda & 1 & 0 & 0 & 0 & 0 & 0 \\ 0 & a_{32} & a_{33} - \lambda & 0 & 0 & 0 & 0 & 0 \\ 0 & 0 & 0 & -\lambda & 1 & 0 & 0 & 0 \\ 0 & 0 & 0 & 0 & -\lambda & 1 & 0 & 0 \\ 0 & 0 & 0 & 0 & 0 & a_{66} - \lambda & 0 & 0 \\ 0 & 0 & 0 & 0 & 0 & 0 & -\lambda & 1 \\ \gamma & 0 & 0 & -\gamma c & 0 & 0 & 0 & a_{88} - \lambda \end{vmatrix} = 0,$$

where

$$\gamma = -\frac{\phi A_2}{A_4}Prh_8,\ a_{32} = \frac{\phi A_1}{A_3}\left(K + \frac{M}{A_1}\right),$$
$$a_{33} = -\frac{\phi A_1}{A_3}(a_1 + ca_4),\ a_{66} = -\frac{\phi A_1}{A_3}(a_1 + ca_4),$$
$$a_{88} = -\frac{\phi A_2}{A_4}Pr(a_1 + ca_4).$$

The characteristic equation becomes

$$\lambda^4(a_{88} - \lambda)(a_{66} - \lambda)\left(\lambda^2 - a_{33}\lambda - a_{32}\right) = 0,\ \lambda_{1,2,3,4} = 0,$$
$$\lambda_5 = a_{88} < 0, \lambda_6 = a_{66} < 0 \text{ provided } a_1 + ca_4 > 0,$$
$$\lambda_{7,8} < 0, \text{ provided } a_{33} < 0,\ a_{32} < 0.$$

Hence, the system is stable provided $a_1 + ca_4 > 0$. The values of the parameters will therefore be chosen so that $a_1 + ca_4 > 0$ and since $\frac{\phi A_1}{A_3}\left(K + \frac{M}{A_1}\right) > 0$, then the values of $M$ and $K$ can be chosen arbitrarily.

## 2.5 Validation of Results

The results obtained in this study are validated with the results obtained using the MATLAB bvp5c solver when $M \to 0$, $K \to 0$. The results are shown in Table 4. There is an excellent agreement between the results. Hence, the bvp4c is used to numerically study the problem under consideration.

# 3. Analysis and Discussion of Results

In the flow under consideration, the ternary hybrid nanofluid is made from the suspension of carbon nanotubes, graphene nanoparticles and $Al_2O_3$ nanoparticles in water base fluid. By rendering the governing equations dimensionless, the flow becomes equipped with some dimensionless parameters. This section discusses the dynamics of the flow as the dimensionless parameters (stretching parameter $c$, suction velocity $f_w$, Coriolis force $K$, magnetic strength $M$, and heat source $Q$) vary during the flow.

## 3.1 Analysis of Results

The flow properties are visualised graphically to illustrate the behaviour of the flow properties (the primary velocity, secondary velocity and temperature) as the flow parameters are varied. Figures (2a) and (2b) visually illustrate the behaviour of the velocity components in the $x$- and $y$-directions. It is observed that the velocity decreases in all directions as the stretching ratio increases. The stretching ratio is varied over the interval $[0.1, 1.0]$ where $c = 0.1$ indicates that stretching in the $x$-direction is faster than stretching in the $y$-direction and $c = 1.0$ indicates that stretching is happening at the same rate in both directions. Similarly, temperature is shown in Figure (2c) to reduce as the stretching ratio increases. The influence of suction velocity $f_w$ (chosen from the interval $[0.1, 0.7]$) on the flow velocity and temperature is shown in Figures (3a), (3b) and (3c). As observed in Figures (3a) and (3b), increasing suction reduces velocity in all directions and Figure (3c) shows that temperature reduces with increasing suction. The effects of Coriolis force, measured by the dimensionless parameter $K$, are studied in Figures (4a) and (4b). By varying the Coriolis force over the interval $K \in [0.01, 1.00]$, where $K = 0.01$ indicates the presence of nearly no rotation while $K = 1.00$ represents a moderately rotating surface. Coriolis force reduces the primary velocity decreases (as shown in Figure (4a)) but increases the secondary velocity (as shown in Figure (4b)). The flow is equipped with some heat source and it is observed in Figure (5) that the temperature of the flow increases as heat source increases.

The skin friction in both $x$- and $y$-directions are displayed in Figures (6a) and (6b) for varying Coriolis force, stretching ratio and heat source. Figure (6a) shows that skin friction in the $x$-direction increases as either Coriolis force or stretching ratio increases. More so, increasing heat source only slightly decreases the skin friction in the $x$-direction. Figure (6b) shows that skin friction in the $y$-direction increases as stretching ratio increases but decreases with increasing Coriolis force. More so, increasing the heat source only slightly increases the skin friction in the $y$-direction. Figure (7) shows the behaviour of heat transfer rate. Increasing the Coriolis force only contributes very slowly to an increase in the heat transfer rate, a higher heat source leads to a reduction in the heat transfer rate and the stretching ratio decreases the heat transfer rate.

## 3.2 Discussion of Results

A summary of the results is provided in Table (1). The results are discussed in this section and our findings are compared with existing literature.

The stretching ratio described by Makhdoum et al. [36] is the ratio of wall stretching in one direction to wall stretching in another direction. In this case, the boundary condition $u(\eta = 0) = axf'(\eta)$ and $v(\eta = 0) = acyg'(\eta)$ gives a stretching ratio $c$. Establishing that the primary direction is the $x$-direction, then the ratio stretching ratio describes the ratio of stretching in the $x$-direction to the stretching in the $y$-direction. The values of $c$ were restricted to the interval $[0.1, 1.0]$ so that the stretching in the $y$-direction is less than or equal to the stretching in the $x$-direction (where equality only holds when $c = 1$). According to the study by Oke [15], the stretching ratio decreases the primary velocity but increases the secondary velocity. However, our results show that both the primary and the secondary velocities are reduced by increasing the stretching ratio. The conflict in the effect of the stretching ratio on the secondary velocity could be due to restrictions placed on the secondary wall so that the secondary wall cannot move faster than the primary wall. The stretching ratio increases the skin friction in all directions but decreases the heat transfer rate. This outcome agrees with the study of Makhdoum et al. [36]. Suction

measures the amount of partial vacuum created when the fluid is drawn towards a region of lower pressure [37]. Makhdoum et al. [37] showed that suction decreases the temperature and this is in agreement with our findings. The partial pressure created by suction leads to a reduction in the thermal energy distribution in the flow and hence, increasing the suction leads to a reduction in the temperature. Coriolis force as described by [12] is the inertia force generated in a rotating system and is responsible for the fictitious deflection of the path of moving objects in the rotating frame. Coriolis force increases as angular velocity increases. As angular velocity increases, the flow experiences sideways lurching to the secondary direction. The dynamic equilibrium is maintained by the reduction in flow in the primary direction [12]. The heat source, measured by the heat source parameter $Q$, represents the external heat source introduced to the flow. Increasing the heat source enhances the inherent thermal energy in the flow and thereby raises the temperature. This finding agrees with that found in the ref [4].

| | $u$ | $v$ | $T$ | $C_{fx}$ | $C_{fy}$ | $Nu$ |
|---|---|---|---|---|---|---|
| $c$ | ↓ | ↓ | ↓ | ↑ | ↑ | ↓ |
| $f_w$ | ↓ | ↓ | ↓ | - | - | - |
| $K$ | ↓ | ↑ | - | ↑ | ↓ | ↑ |
| $Q$ | - | - | ↑ | ↓ | ↑ | ↓ |

Table 1: Summary of analysis

## 4. Conclusion

This work analyses the flow of ternary hybrid nanofluid obtained by the suspension of graphene and alumina nanoparticles in water. The flow is subjected to some heat source while the wall of the channel is moveable and rotating. The flow equations are developed, rendered dimensionless and simulated to illustrate the effects of various parameters. The main outcomes of the study include;

- The stretching ratio reduces flow temperature, velocity in all directions and heat transfer rate but increases the skin friction in all directions.
- Heat transfer rate is enhanced with increasing Coriolis force.
- Increasing rotation leads to an increase in both the skin friction in the primary flow direction and the heat transfer rate but a reduction in the skin friction in the secondary flow direction.
- More heat source increases flow temperature and secondary skin friction but decreases primary skin friction and heat transfer rate.

This study focuses on flows subject to a low to moderately high rotation, excluding extremely high rotation. In instances of high rotation, the fluid dynamics becomes turbulent. Examining the behaviour of hybrid ternary fluid flow over a rapidly rotating surface could be of scientific interest, offering insight into a domain characterized by turbulent fluid dynamics. This study has emphasised on using similar nanoparticle shapes, and some other works of literature (see [38, 39, 13, 33]) have emphasised dissimilar nanoparticles. It will be of benefit to the industry if comparisons between flows of ternary hybrid nanofluid with similar and dissimilar nanoparticle shapes can be made.

### *References*

[1] James Clerk Maxwell. A Treatise on Electricity and Magnetism. *Nature*, 7:478–480, 1873. doi: https://doi.org/10.1038/007478a0.

[2] Stephen U. S. Choi and J. A. Eastman. Enhancing Thermal Conductivity of Fluids with Nanoparticles. *ASME International Mechanical Engineering Congress & Exposition*, 1995.

[3] John Kinyanjui Kigio, Mutuku Winifred Nduku, and Oke Abayomi Samuel. Analysis of Volume Fraction and Convective Heat Transfer on MHD Casson Nanofluid over a Vertical Plate. *Fluid Mechanics*, 7(1):1–8, 2021. doi: 10.11648/j.fm.20210701.11.

[4] A. S. Oke, I. L. Animasaun, W. N. Mutuku, M. Kimathi, Nehad Ali Shah, and S. Saleem. Significance of Coriolis force, volume fraction, and heat source/sink on the dynamics of water conveying 47Â nm

alumina nanoparticles over a uniform surface. *Chinese Journal of Physics*, 71:716–727, 2021. ISSN 0577-9073. doi: https://doi.org/10.1016/j.cjph.2021.02.005.

[5] S. Lee, S. U.-S. Choi, S. Li, and J. A. Eastman. Measuring Thermal Conductivity of Fluids Containing Oxide Nanoparticles. *Journal of Heat Transfer*, 121(2):280–289, may 1999. doi: 10.1115/1.2825978.

[6] Mohammadali Baghbanzadeh, Alimorad Rashidi, Davood Rashtchian, Roghayeh Lotfi, and Azadeh Amrollahi. Synthesis of spherical silica/multiwall carbon nanotubes hybrid nanostructures and investigation of thermal conductivity of related nanofluids. *Thermochimica Acta*, 549:87–94, dec 2012. doi: 10.1016/j.tca.2012.09.006.

[7] S. Suresh, K. P. Venkitaraj, P. Selvakumar, and M. Chandrasekar. Effect of Al2O3-Cu/water hybrid nanofluid in heat transfer. *Experimental Thermal and Fluid Science*, 38:54–60, apr 2012. doi: 10.1016/j.expthermflusci.2011.11.007.

[8] Tanzila Hayat and S. Nadeem. Heat transfer enhancement with Ag-CuO/water hybrid nanofluid. *Results in Physics*, 7: 2317–2324, 2017. ISSN 2211-3797. doi: 10.1016/j.rinp.2017.06.034.

[9] A. S. Oke, B. C. Prasannakumara, W. N. Mutuku, R. J. Punith Gowda, B. A. Jumaand R. Naveen Kumar, and O. I. Bada. Exploration of the effects of Coriolis force and thermal radiation on water-based hybrid nanofluid flow over an exponentially stretching plate. *Scientific Reports*, 12(1), December 2022. ISSN 2045-2322. doi: 10.1038/s41598-022-21799-9.

[10] K. Thriveni and B. Mahanthesh. Sensitivity analysis of nonlinear radiated heat transport of hybrid nanoliquid in an annulus subjected to the nonlinear Boussinesq approximation. *Journal of Thermal Analysis and Calorimetry*, 143(3):2729–2748, apr 2020. doi: 10.1007/s10973-020-09596-w.

[11] K. Thriveni and B. Mahanthesh. Sensitivity computation of nonlinear convective heat transfer in hybrid nanomaterial between two concentric cylinders with irregular heat sources. *International Communications in Heat and Mass Transfer*, 129:105677, dec 2021. doi: 10.1016/j.icheatmasstransfer.2021.105677.

[12] Abayomi Samuel Oke. Combined effects of Coriolis force and nanoparticle properties on the dynamics of gold-water nanofluid across nonuniform surface. *ZAMM - Journal of Applied Mathematics and Mechanics / Zeitschrift fÃŒr Angewandte Mathematik und Mechanik*, 0(0):e202100113, 2022. doi: https://doi.org/10.1002/zamm.202100113.

[13] Thanaa Elnaqeeb, Isaac Lare Animasaun, and Nehad Ali Shah. Ternary-hybrid nanofluids: significance of suction and dual-stretching on three-dimensional flow of water conveying nanoparticles with various shapes and densities. *Zeitschrift für Naturforschung A*, 76(3):231–243, 2021. doi: doi:10.1515/zna-2020-0317. URL `https://doi.org/10.1515/zna-2020-0317`.

[14] S. M. Mousavi, F. Esmaeilzadeh, and X. P. Wang. Effects of temperature and particles volume concentration on the thermophysical properties and the rheological behavior of CuO/MgO/TiO2 aqueous ternary hybrid nanofluid. *Journal of Thermal Analysis and Calorimetry*, 137(3):879–901, jan 2019. doi: 10.1007/s10973-019-08006-0.

[15] Abayomi Samuel Oke. Heat and Mass Transfer in 3D MHD Flow of EG-Based Ternary Hybrid Nanofluid Over a Rotating Surface. *Arabian Journal for Science and Engineering*, 2022. ISSN 2191-4281. doi: 10.1007/s13369-022-06838-x. URL `https://doi.org/10.1007/s13369-022-06838-x`.

[16] Nadeem Abbas, S. Nadeem, Anber Saleem, M. Y. Malik, Alibek Issakhov, and Fahd M. Alharbi. Models base study of inclined MHD of hybrid nanofluid flow over nonlinear stretching cylinder. *Chinese Journal of Physics*, 69:109–117, 2021. ISSN 0577-9073. doi: https://doi.org/10.1016/j.cjph.2020.11.019.

[17] Nur Syazana Anuar, Norfifah Bachok, and Ioan Pop. Cu-Al2O3/Water Hybrid Nanofluid Stagnation Point Flow Past MHD Stretching/Shrinking Sheet in Presence of Homogeneous-Heterogeneous

and Convective Boundary Conditions. *Mathematics*, 8(8), 2020. ISSN 2227-7390. doi: 10.3390/math8081237. URL https://www.mdpi.com/2227-7390/8/8/1237.

[18] Nirmalendu Biswas, U. K. Sarkar, Ali J. Chamkha, and Nirmal Kumar Manna. Magneto-hydrodynamic thermal convection of Cu-Al2O3/water hybrid nanofluid saturated with porous media subjected to half-sinusoidal nonuniform heating. *Journal of Thermal Analysis and Calorimetry*, 143(2):1727–1753, January 2021. ISSN 1588-2926. doi: 10.1007/s10973-020-10123-0.

[19] Iskander Tlili, Hossam A. Nabwey, M. Girinath Reddy, N. Sandeep, and Maddileti Pasupula. Effect of resistive heating on incessantly poignant thin needle in magneto-hydrodynamic Sakiadis hybrid nanofluid. *Ain Shams Engineering Journal*, 12(1): 1025–1032, 2021. ISSN 2090-4479. doi: https://doi.org/10.1016/j.asej.2020.09.009.

[20] Abayomi S. Oke, Winifred N. Mutuku, Mark Kimathi, and Isaac Lare Animasaun. Coriolis effects on MHD newtonian flow over a rotating non-uniform surface. *Proceedings of the Institution of Mechanical Engineers, Part C: Journal of Mechanical Engineering Science*, 235(19):3875–3887, 2021. doi: 10.1177/0954406220969730. URL https://doi.org/10.1177/0954406220969730.

[21] Anselm O. Oyem, Winifred N. Mutuku, and Abayomi S. Oke. Variability effects on magnetohydrodynamic for Blasius and Sakiadis flows in the presence of Dufour and Soret about a flat plate. *Engineering Reports*, 2(10):e12249, aug 2020. doi: 10.1002/eng2.12249.

[22] Ephesus Olusoji Fatunmbi, Hammed Abiodun Ogunseye, and Precious Sibanda. Magnetohydrodynamic micropolar fluid flow in a porous medium with multiple slip conditions. *International Communications in Heat and Mass Transfer*, 115:104577, jun 2020. doi: 10.1016/j.icheatmasstransfer.2020.104577.

[23] J. O. Ouru, W. N. Mutuku, and A. S. Oke. Buoyancy-Induced MHD Stagnation Point Flow of Williamson Fluid with Thermal Radiation. *Journal of Engineering Research and Reports*, pages 9–18, mar 2020. doi: 10.9734/jerr/2020/v11i417065.

[24] Ephesus Olusoji Fatunmbi, Fazle Mabood, Hedi Elmonser, and Iskander Tlili. Magnetohydrodynamic nonlinear mixed convection flow of reactive tangent hyperbolic nano fluid passing a nonlinear stretchable surface. *Physica Scripta*, 96(1):015204, nov 2020. doi: 10.1088/1402-4896/abc3e9.

[25] Abayomi S. Oke and Winifred N. Mutuku. Significance of viscous dissipation on MHD Eyring–Powell flow past a convectively heated stretching sheet. *Pramana*, 95(4), nov 2021. doi: 10.1007/s12043-021-02237-3.

[26] Belindar A. Juma, Abayomi S. Oke, Winifred N. Mutuku, Afolabi G. Ariwayo, and Olum J. Ouru. Dynamics of Williamson fluid over an inclined surface subject to Coriolis and Lorentz forces. *Engineering and Applied Science Letter*, 5(1):37–46, March 2022. ISSN 2617-9709. doi: 10.30538/psrp-easl2022.0083.

[27] Chiaki Kobayashi, Amanda I. Karakas, and Maria Lugaro. The Origin of Elements from Carbon to Uranium. *The Astrophysical Journal*, 900(2):179, September 2020. ISSN 1538-4357. doi: 10.3847/1538-4357/abae65.

[28] Xiaohui Ye, Ming Qi, Mengzhen Chen, Lihui Zhang, and Jinying Zhang. Zero to three dimension structure evolution from carbon allotropes to phosphorus allotropes. *Advanced Materials Interfaces*, 10 (5), December 2022. ISSN 2196-7350. doi: 10.1002/admi.202201941.

[29] Jiaqiang Li and Yu Han. Artificial carbon allotrope $\gamma$-graphyne: Synthesis, properties, and applications. *Giant*, 13:100140, March 2023. ISSN 2666-5425. doi: 10.1016/j.giant.2023.100140.

[30] Leandro NicolÃ¡s Sacco and Sten Vollebregt. Overview of engineering carbon nanomaterials such as carbon nanotubes (cnts), carbon nanofibers (cnfs), graphene and nanodiamonds and other carbon allotropes inside porous anodic alumina (paa) templates. *Nanomaterials*, 13

(2):260, January 2023. ISSN 2079-4991. doi: 10.3390/nano13020260.

[31] L. Prandtl. "Über Flüssigkeitsbewegung bei sehr kleiner Reibung" translated to "Motion of fluids with very little viscosity". *Int. Math.-Kongr. Heidelb.*, 8(13):1–8, 1904.

[32] B. C. Sakiadis. Boundary layer behavior on continuous solidsurfaces: The boundary layer on a continuous flat surface. *Am.Inst. Chem. Eng. (AIChE)*, 7:221–225, 1961.

[33] Abayomi S. Oke, Ephesus O. Fatunmbi, Isaac L. Animasaun, and Belindar A. Juma. Exploration of ternary-hybrid nanofluid experiencing Coriolis and Lorentz forces: case of three-dimensional flow of water conveying carbon nanotubes, graphene, and alumina nanoparticles. *Waves in Random and Complex Media*, pages 1–20, September 2022. ISSN 1745-5049. doi: 10.1080/17455030.2022.2123114.

[34] A. S. Oke. Convergence of differential transform method for ordinary differential equations. *Journal of Advances in Mathematics and Computer Science*, 24(6):1–17, 2017.

[35] L. F. Shampine, M. W. Reichelt, and J. Kierzenka. Solving Boundary Value Problems for Ordinary Differential Equations in MATLAB with bvp4c. 2010.

[36] Basim M. Makhdoum, Zafar Mahmood, Bandar M. Fadhl, Musaad S. Aldhabani, Umar Khan, and Sayed M. Eldin. Significance of entropy generation and nanoparticle aggregation on stagnation point flow of nanofluid over stretching sheet with inclined Lorentz force. *Arabian Journal of Chemistry*, 16(6):104787, June 2023. ISSN 1878-5352. doi: 10.1016/j.arabjc.2023.104787.

[37] Basim M. Makhdoum, Zafar Mahmood, Umar Khan, Bandar M. Fadhl, Ilyas Khan, and Sayed M. Eldin. Impact of suction with nanoparticles aggregation and Joule heating on unsteady MHD stagnation point flow of nanofluids over horizontal cylinder. *Heliyon*, 9(4):e15012, April 2023. ISSN 2405-8440. doi: 10.1016/j.heliyon.2023.e15012.

[38] I. L. Animasaun, A. S. Oke, Qasem M. Al-Mdallal, and A. M. Zidan. Exploration of water conveying carbon nanotubes, graphene, and copper nanoparticles on impermeable stagnant and moveable walls experiencing variable temperature: thermal analysis. *Journal of Thermal Analysis and Calorimetry*, 148 (10):4513–4522, March 2023. ISSN 1588-2926. doi: 10.1007/s10973-023-11997-6.

[39] Wenhao Cao, Animasaun I. L., Se-Jin Yook, Oladipupo V. A., and Xianjun Ji. Simulation of the dynamics of colloidal mixture of water with various nanoparticles at different levels of partial slip: Ternary-hybrid nanofluid. *International Communications in Heat and Mass Transfer*, 135:106069, jun 2022. doi: 10.1016/j.icheatmasstransfer.2022.106069.

# Appendix

Table 2: **Nomenclature**

| Dimensional quantities | | | |
|---|---|---|---|
| $x, y, z$ | Distance in three-dimensional space $(L)$ | $\sigma$ | electrical conductivity $(M^{-1}L^{-3}T^{3}A^{2})$ |
| $u, v, w$ | Velocity component in the $x, y, z$-directions $(LT^{-1})$ | $\alpha$ | thermal diffusivity $(L^{2}T^{-1})$ |
| $T$ | Dimensional fluid temperature $(K)$ | $B_0$ | magnetic field strength $(L^{-1}A)$ |
| $T_w$ | wall temperature $(K)$ | $\kappa$ | thermal conductivity $(K^{-1})$ |
| $T_\infty$ | free stream temperature $(K)$ | $\rho$ | density $(ML^{-3})$ |
| $c_p$ | Specific heat capacity $(L^{2}T^{-2}K^{-1})$ | $\Omega$ | angular velocity of the surface $(T^{-1})$ |
| $\nu$ | kinematic viscosity $(L^{2}T^{-1})$ | $\mu$ | dynamic viscosity $(ML^{-1}T^{-1})$ |

| Dimensionless quantities | | | |
|---|---|---|---|
| $f'$ | primary velocity | $K$ | rotation parameter |
| $g'$ | secondary velocity | $Pr$ | Prandtl number |
| $\Theta$ | temperature | $f_w$ | suction |
| $M$ | Magnetic field parameter | $c$ | stretching ratio |
| $C_{fx}$ | local skin friction in $x$-direction | $\phi$ | volume fraction |
| $Q$ | Heat source parameter | $N_{ux}$ | Nusselt number in $x$-direction |
| $C_{fy}$ | local skin friction in $y$-direction | $N_{uy}$ | Nusselt number in $y$-direction |

| Subscripts | | | |
|---|---|---|---|
| $tf$ | ternary hybrid nanofluid | $bf$ | base fluid |
| $1, 2, 3$ | CNT, graphene, $Al_2O_3$ nanoparticle | | |

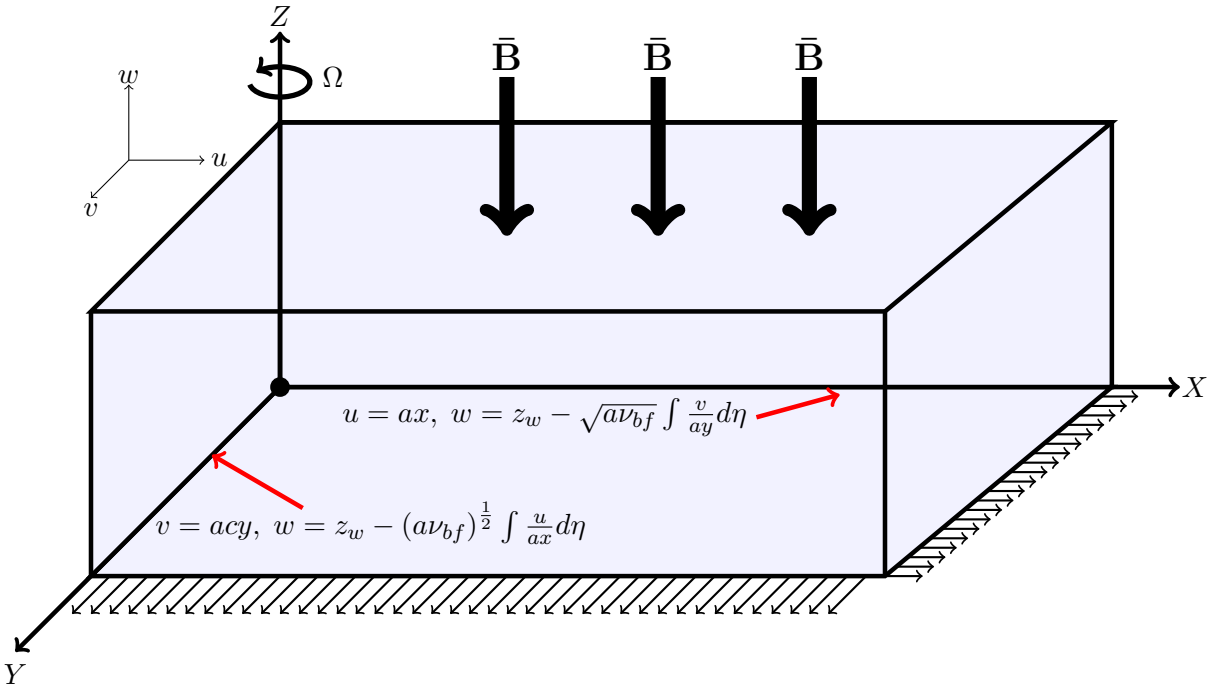


Figure 1: Flow configuration

Table 3: thermal and physical properties [20]

| | $\rho\left(kgm^{-3}\right)$ | $k\left(Wm^{-1}K^{-1}\right)$ | $c_p\left(Jkg^{-1}K^{-1}\right)$ |
|---|---|---|---|
| carbon nanotubes | 2100 | 3007.4 | 410 |
| graphene | 2200 | 5000 | 790 |
| $Al_2O_3$ | 3970 | 40 | 765 |
| water | 997.1 | 0.613 | 4179 |

Table 4: Results Validation for $M = K = 0, f_w = 0.3, Pr = 6.2, \eta_\infty = 70$

| $c$ | $Q$ | $f''(0)$ | | $g''(0)$ | | $\Theta'(0)$ | |
|---|---|---|---|---|---|---|---|
| | | bvp4c | bvp5c | bvp4c | bvp5c | bvp4c | bvp5c |
| 5.0 | 0.1 | -0.6751 | -0.6727 | -0.9173 | -0.9138 | 2.7848 | -2.7685 |
| 5.5 | 0.1 | -0.6943 | -0.6918 | -0.9568 | -0.9531 | 2.8759 | -2.858 |
| 6.0 | 0.1 | -0.713 | -0.7102 | -0.9946 | -0.9907 | 2.9636 | -2.9441 |
| 0.3 | 0.5 | -0.443 | -0.4422 | -0.3553 | -0.3549 | 1.09 | -1.0905 |
| 0.3 | 1.0 | -0.443 | -0.4422 | -0.3553 | -0.3549 | 0.4711 | -0.4717 |
| 0.3 | 1.5 | -0.443 | -0.4422 | -0.3553 | -0.3549 | -0.1478 | 0.1472 |

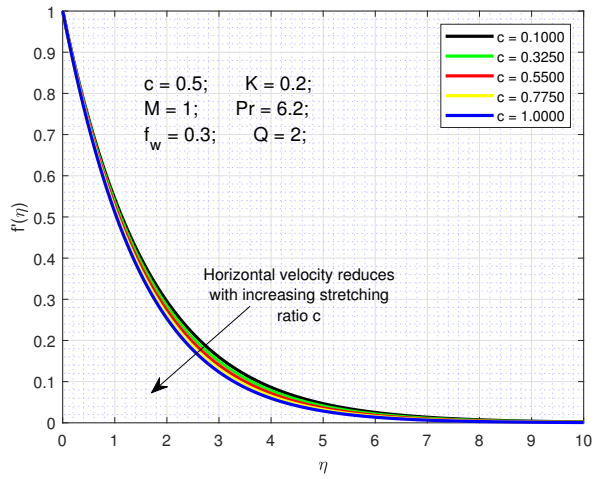


(a) primary velocity with stretching ratio

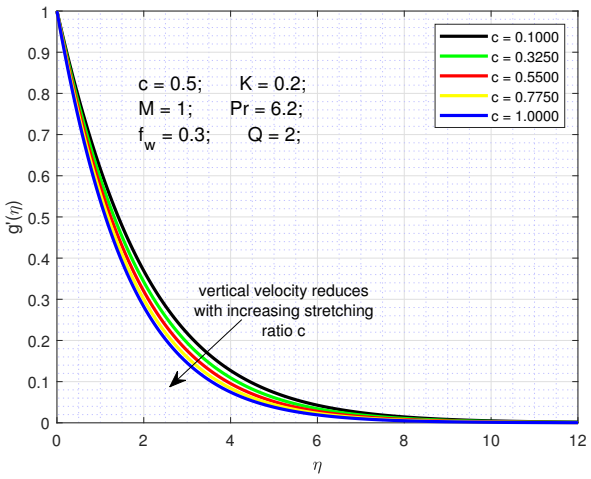


(b) secondary velocity with stretching ratio

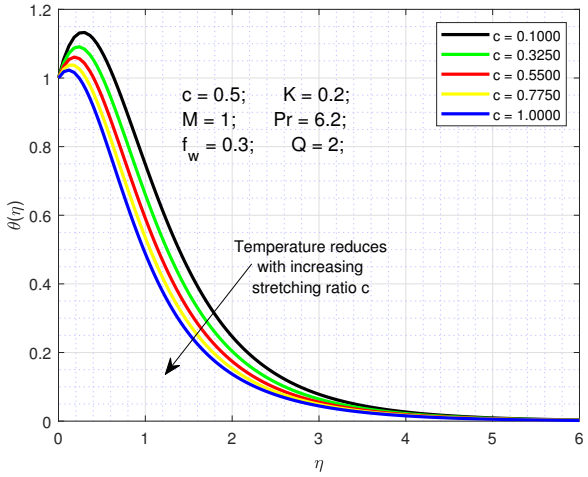


(c) temperature with stretching ratio

Figure 2: stretching ratio effects

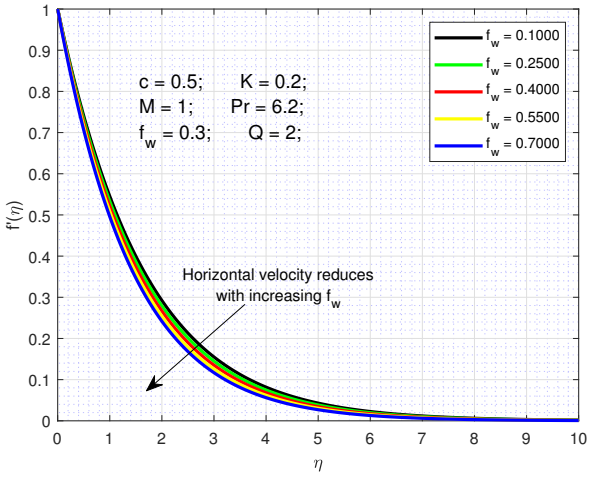


(a) primary velocity with suction

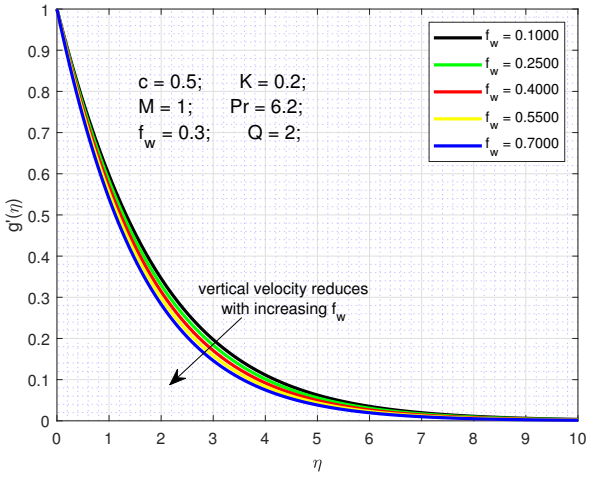


(b) secondary velocity with suction

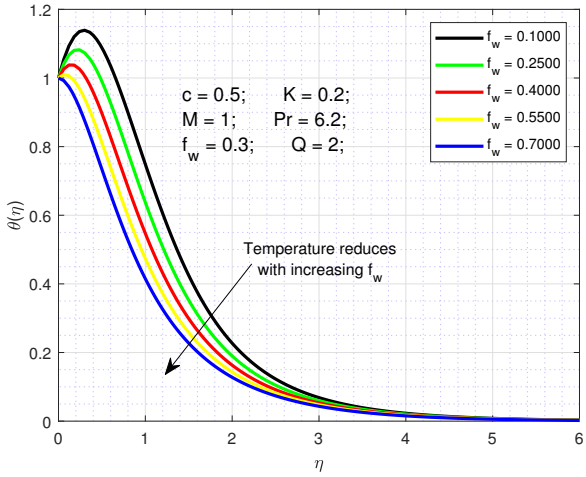


(c) temperature with suction

Figure 3: suction effects

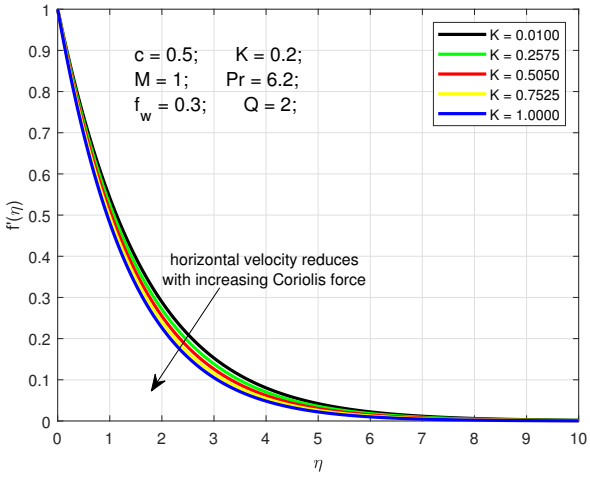


(a) primary velocity with Coriolis force

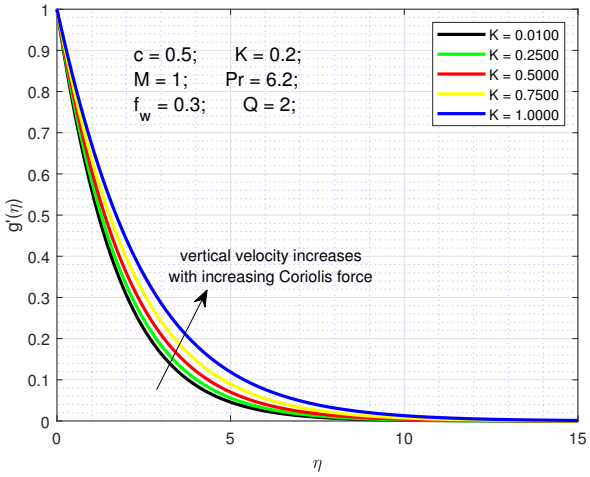


(b) secondary velocity with Coriolis force

Figure 4: Coriolis force effect

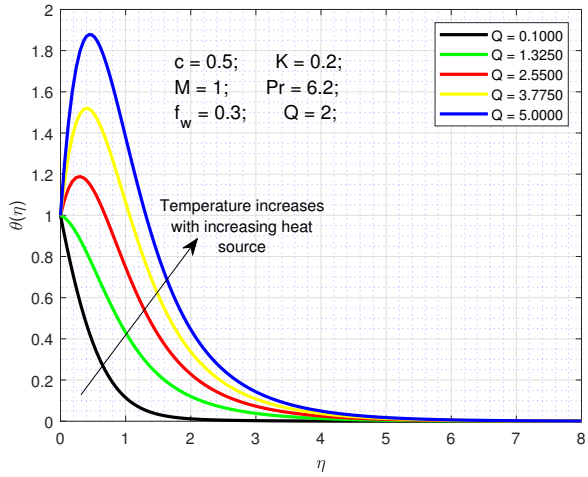


Figure 5: temperature with heat source

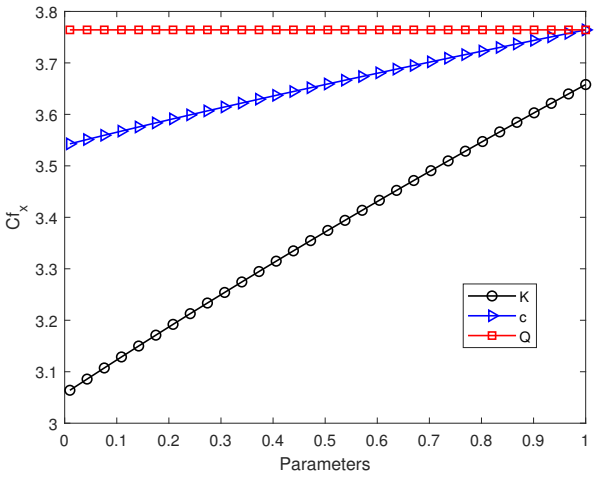


(a) skin friction in $x$-direction

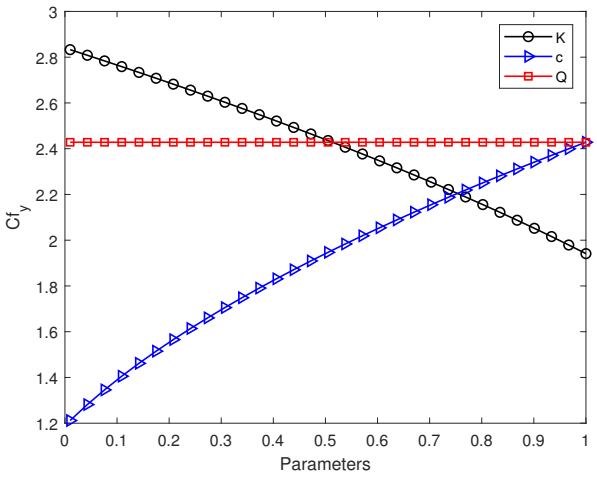


(b) skin friction in $y$-direction

Figure 6: skin friction

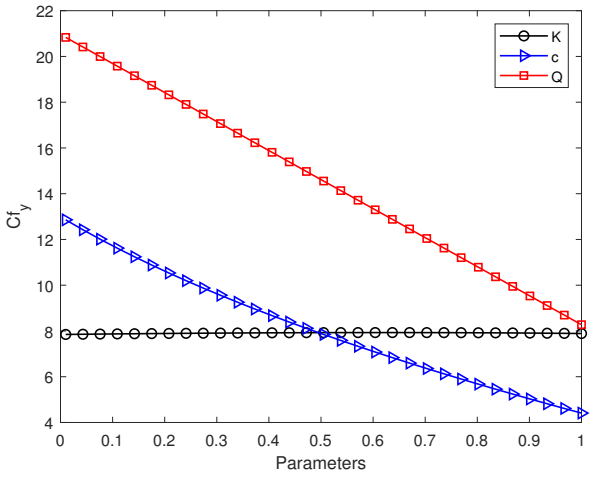


Figure 7: heat transfer rate